J. Vis. Commun. Image R. 24 (2013) 739–751

Contents lists available at SciVerse ScienceDirect

J. Vis. Commun. Image R.

journal homepage: www.elsevier.com/locate/jvci

# RII: Renovating the irregular illumination of digital image archives

Jung-San Lee

*Department of Information Engineering and Computer Science, Feng Chia University, Taichung 40724, Taiwan, ROC*

ARTICLE INFO

*Article history:*
Received 13 October 2012
Accepted 3 May 2013
Available online 15 May 2013

*Keywords:*
Digital archive
Under-exposure
Over-exposure
Illumination
Distortion
Gauss–Laplace
Radiance
Edge detection

ABSTRACT

Digitization is critical for preserving valuable culture archives such as texts and images. Considering the physical characters of digital cameras or scanners and the artificial negligence, some distortions such as under-exposure or over-exposure often appear in the digital form of archives. These distortions decrease the quality of the digital pieces and lead to disputation in some circumstances. Several methods have been used to deal with these illumination problems. These existing methods mainly focus on how to mitigate the under-exposure phenomenon in text-only or text-photo images. Over-exposure cases in which brightness comes from different orientations are not considered. Hence, we propose a novel system for renovating irregular illumination (RII) to handle the over-exposure problem as well as under-exposure distortion. Experimental results show that the processing outcomes of RII can guarantee accurate restoration of the transformed digital pieces. In particular, RII can be extended to improve the uneven light distribution problem for complicated and colorful images.



## 1. Introduction

Due to the rapid development of this information society, it is important to convert works securely, quickly, and conveniently into digital forms using highly developed science and technology [1]. Digitization is critical for preserving culture and protecting valuable information. It is essential for active participation in government and in various academic organizations, which make up a large part of our society. However, there still exist some tough problems within this process. Considering the characters of tools such as cameras or scanners, environmental factors, and the artificial negligence, illumination of digital photos or scanned images is often unevenly distributed after conversion [2–5]. This leads to distortion of the content of the image and degrades the quality of primary text or text-photo objects. Thus, finding an efficient way to solve this problem in order to achieve the goal of transforming original materials into their digital forms without distorting the content or losing their essential characters is quite significant [6]. Motivated by this, many researchers aim to balance the irregular radiance of transformed archive to obtain accurate results.

Hsia and Tsai propose an efficient light-balancing technique (ELBT) that aims to perfectly adjust the illumination of text images [7]. Nevertheless, ELBT can only handle problems in text-only pieces and becomes invalid for images with text-photo objects. Hsia et al. provide a line-based light balancing technique (LLBT), which improves the illumination adjustment [8]. Hsia et al. also offer a diverse LLBT method to stabilize the light of a photo image; unfortunately, this method fails when dealing with text-only images Lee et al. manipulate the Sobel mechanism to develop an illumination balance technique (SIBT) for both text-only and text-photo images [9]. Although SIBT can adjust the illumination of objects inside the under-exposure images according to the light distribution of the whole background, and thus outperform ELBT and LLBT, it is still invalid for images with over-exposure.

In fact, it is common to obtain an over-exposure image when using a camera to convert an archive into digital form, especially when the digitizing process needs the help of a flash or stays under the heavy sunshine. Existing illumination mechanisms are unable to balance the radiance distribution of both text and text-photo images for under-exposure and over-exposure atmospheres. In this paper, we propose a novel system for renovating irregular illumination (RII) to improve the quality of under-exposure/over-exposure images containing both text and text-photo objects. The strategy is to judge the radiance distribution in order to determine whether the image has under-exposure or over-exposure, which allows us to deal with the two kinds of distorted images. Then, we employ the Gauss–Laplace detector to help contour the objects; based on this, we can sign out the objects within images [10,11]. This edge-detecting mechanism can also perform well on images with JPEG or other noise-adding attacks, because the objects can be easily signed out. We separate these objects as texts and photos to further dispose them with different techniques.

While processing various kinds of images, the simulation results show that RII is superior to ELBT, LLBT, and SIBT in balancing the radiance of a degraded image with text and text-photo materials inside. RII can handle both under-exposure text and text-photo images with higher visual quality and can also improve over-exposure. In order to evaluate the performance of these mechanisms,

*E-mail address:* leejs@fcu.edu.tw

1047-3203/$ - see front matter © 2013 Elsevier Inc. All rights reserved.
http://dx.doi.org/10.1016/j.jvcir.2013.05.002

we apply the peak signal-to-noise rate (*PSNR*) for artificial images in order to show the effects within the experiments [12–14]. Displaying a much higher *PSNR* value than others when processing the under-exposure images, RII demonstrates its efficiency. Furthermore, managing the over-exposure images stably with a *PSNR* value of more than 24 dB, RII proves its satisfactory effect for the human visual system. Additionally, we employ the light drift level (*LDL*) value to demonstrate the light distribution of the proposed method [8]. Regarding these characters, RII can improve the distorted transformed archive and enhance its quality. In particular, RII can be extended to balance the uneven light distribution problem for colorful images.

The rest of this paper is organized as follows. In Section 2, we describe a detailed method of RII to show how it works, followed by the experimental results and discussions shown in Section 3. Experiments for complicated and colorful images are given in Section 4. Then we make conclusions in Section 5.

## 2. Renovating irregular illumination technique

In this section, we describe how the proposed method can deal with the irregular radiance problem for both over-exposure and under-exposure images. There are eight phases in this method: estimating light degree, detecting edge, signing objects, evaluating light distribution, balancing radiance, separating texts from photos, balancing texts, and balancing photos. The outcome of each step is displayed in Fig. 1. Additionally, a simulator $T$ is employed to help introduce the procedure in detail. The first phase is used to estimate the light degree of two types of target images. Then, we can determine whether the input image has under-exposure or over-exposure. As the illumination balance of the object is distinct from that of the background, we have to separate the text and photo objects from the background. Thus, we need to detect the edges to draw the contour of all objects. Next, we transform the result into a binary image to help mark all objects. Finally, we can handle both kinds of images with the proper steps.

### 2.1. Estimating light degree

In this phase, the transformed pieces of the archive can be classified as over-exposure or under-exposure according to the pixel values within the image, as shown in Fig. 1(a) and (b). To determine the radiance distribution level of the target image, we employ pixels on four corners of the squares to evaluate the performance of the whole image; these pixels are defined as corner pixels ($CP(j), j = 1,2,3,4$). Then we have an assessment value $AV_i$ of the $i$th square, which is defined as

$$AV_i = \begin{cases} 1, & \text{if} \quad \frac{1}{4}\sum_{j=1}^{4} CP(j) \geq 200 \\ 0, & \text{if} \quad \frac{1}{4}\sum_{j=1}^{4} CP(j) < 200 \end{cases}. \tag{1}$$

The number of squares can be adjusted according to the different sizes of the diverse images. We then apply $ST$ squares of $4 \times 4,\ 8 \times 8,\ 16 \times 16,\ 32 \times 32,\ 64 \times 64, \ldots, N \times N$ to compute the determination pixel ($DP$) as follows. Here, $AV_i$ is used to help determine the selected square belonging to the over-exposure or under-exposure set. When all of the $AV$ values have been obtained, the final decision can be made through the voting rule:

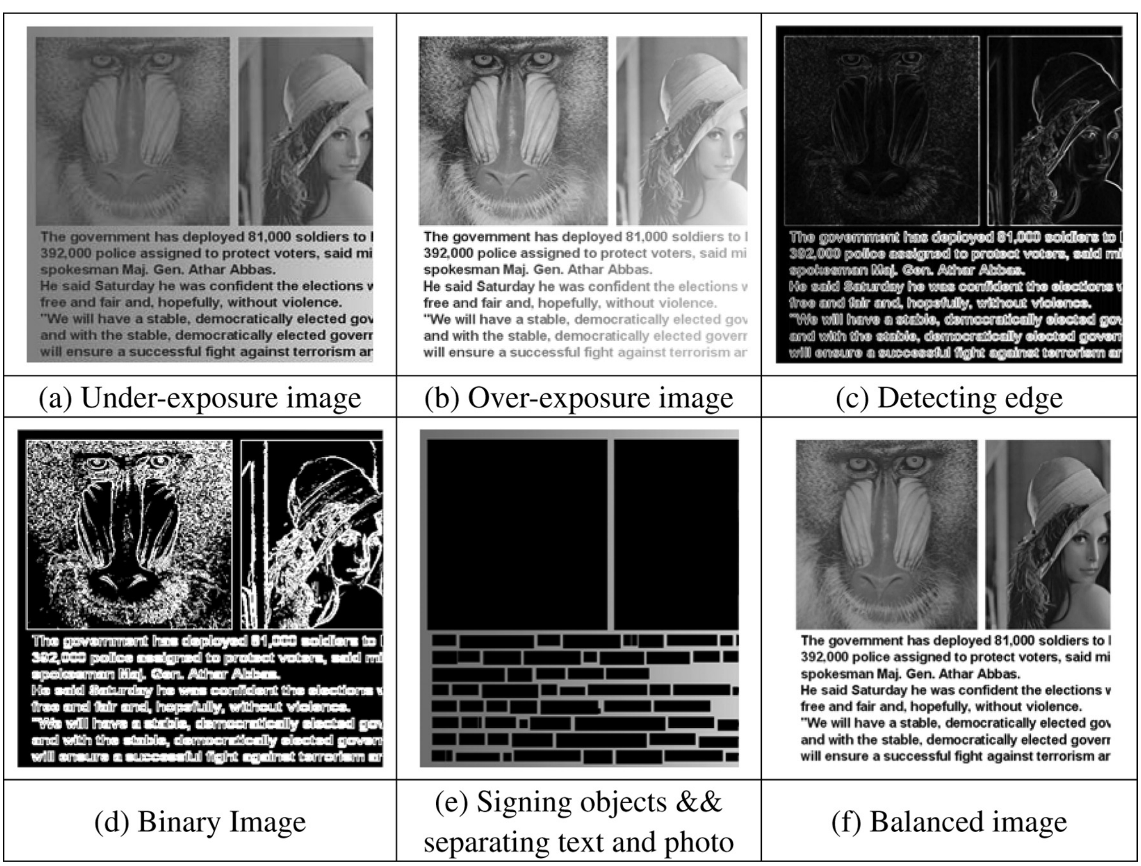


**Fig. 1.** Flowchart of RII.

$$DP = \sum_{i=1}^{ST} AV_i - \frac{1}{2}ST, \tag{2}$$

where $ST$ is the total number of the employed squares. If the $DP$ is equal or greater than zero, the processed image can be classified as over-exposure; otherwise, it is regarded as under-exposure. As the under-exposure or over-exposure phenomenon often occurs in the edges, it is efficient to make use of the points on the corner, which are the intersection part of the edges, to evaluate the performance of the image.

Furthermore, as the selected squares range from center to the outside, $T$ can judge whether the image is under-exposure or over-exposure no matter from where the distortions come. Considering the values obtained from theses squares, we apply the voting rule here to determine the light distribution of the sample image. If half and more than half of the values show over-exposure, then the sample is defined as over-exposure. Even the imbalanced radiance only takes a little part of the whole image; it is still possible to detect the imbalance factor, since the normal values should not contribute anything to the computation of $DP$. Here, the threshold of $CP$ is set as 200, which is a little high in average images. If the computed $CP$ value is a normal one, it is put into the under-exposure set. Considering that the process for under-exposure images is also suitable for normal images, other samples can be dealt with in this way, except for over-exposure samples. Thus, sample images can be repaired separately based on the radiance level within the image.

### 2.2. Detecting edge

In this phase, we draw the edge of all objects in the image. The Gauss–Laplace detector is shown in Fig. 2. Simulator $T$ applies these detectors to help draw the edge and construct the five edge maps $EM_1$, $EM_2$, $EM_3$, $EM_4$, and $EM_5$. These edges are then used to generate an average edge map $EM_{avg}$, as illustrated in Fig. 1(c) [11]. Here, $PT$ represents the pre-defined threshold, which is used to build a binary image. Based on $PT$, $T$ transforms $EM_{avg}$ into a binary edge map $BM$, as displayed in Fig. 1(d). The Gauss–Laplace detector is a kind of the second derivative operator. It detects edges by computing the second derivative zero-crossing value in the gray-scale image. In order to get rid of noise, it uses the Gaussian function to filter the obtained wave and then calculates the second derivative.

First, $T$ employs the Gauss–Laplace method to bolder the edge of the original image. The pixel value within $EM_{avg}$ is calculated as

$$EM_{avg}(px_i) = \frac{1}{5}\sum_{n=1}^{5}\sum_{i=1}^{h\times w} EM_n(px_i), \tag{3}$$

where $px_i$ is the pixel value in $EM_{avg}$. To make the process more convenient, pixels in $EM_{avg}$ are computed referring to the Gauss–Laplace detector.

Finally, simulator $T$ converts the average edge map $EM_{avg}$ into the corresponding binary image referring to the pre-defined threshold $PT$. If $EM_{avg}(px_i) \geq PT$, then $EM_{avg}(px_i) = 255$; otherwise, $EM_{avg}(px_i) = 0$, where $i = 0, 1, \ldots, w \times h$, where $EM_{avg}(px_i)$ denotes the $i$th pixel values of $EM_{avg}$, $h$ and $w$ represent the height and width of sampling image. Thus, the binary image is obtained.

$$\begin{bmatrix} 0 & -1 & 0 \\ -1 & 4 & -1 \\ 0 & -1 & 0 \end{bmatrix}, \begin{bmatrix} -1 & -1 & -1 \\ -1 & 8 & -1 \\ -1 & -1 & -1 \end{bmatrix}, \begin{bmatrix} 0 & 1 & 0 \\ 1 & -4 & 1 \\ 0 & 1 & 0 \end{bmatrix}, \begin{bmatrix} 1 & 1 & 1 \\ 1 & -8 & 1 \\ 1 & 1 & 1 \end{bmatrix}, \begin{bmatrix} -1 & 2 & -1 \\ 2 & -4 & 2 \\ -1 & 2 & -1 \end{bmatrix}$$

**Fig. 2.** Gauss–Laplace detector.

### 2.3. Signing objects

To locate texts and photos in sampling image $M$, simulator $T$ marks them with squares to form the signed image, which is depicted in Fig. 1(e). Here, we illustrate this process step by step:

Step 1. For the binary image $BM$, if $EM_{avg}(px_i) = 255$, add $M(p_i)$, which stands for the $i$th location of $M$, to the set of coordinates $S_j$. Otherwise, go to Step 5. Note that $S_j$ belongs to the object $j$.
Step 2. Compare four neighbors (up, down, left, right) of the unchecked $M(p_i)$ in $S_j$. If the neighbor is not in $S_j$ and its pixel value is 255, add this neighbor into $S_j$.
Step 3. Repeat Step 2 until no more points can be added to $S_j$.
Step 4. List the highest, lowest, leftmost, and rightmost coordinates in $S_j$, and then sign a square in $M$ referring to these coordinates. Set all pixels within the signed square in $BM$ as zero.
Step 5. Refresh $i = i + 1$. Repeat Steps 1–4 until $i = w \times h$.

### 2.4. Evaluating light distribution

In this phase, simulator $T$ helps to generate a light distribution image $LDM$ from the signed image. To find signed sections, $T$ examines every pixel from the signed image. It is obvious that a signed section is a vertical line with connected signed pixels.

First, $T$ vertically checks the signed section in the signed image from column to column. During this process, if a signed section is found, $T$ records the first and last locations of this line as $l_f$ and $l_l$. Next, $T$ interpolates pixels of the signed section in the direction of line as

$$LDM(px_{f+k-1}) = M(px_{f-1}) + [M(px_{l+1}) - M(px_{f-1})/m] \times k, \tag{4}$$

where $k$ is the $k$th pixel and $m$ is the total number of pixels in the signed section.

Subsequently, $T$ repeats the procedure mentioned above until all signed sections have been handled. Then, we can obtain the light distribution image of the transformed piece, by which the background light can be balanced to display the original color.

### 2.5. Balancing radiance

To recover and complete the background illumination, we adjust the whole background pixel values based on the light distribution image ($LDM$). Due to the light distribution image $LDM$, simulator $T$ can balance the illumination of the original sampling image $M$.

If $M(px_i)$ is a signed location, $T$ adjusts $M(px_i)$ as follows:

$$M(px_i') = (260/LDM(px_i)) \times M(px_i), \tag{5}$$

where the value 260 is suggested by [9] and used to determine the illumination of the processed image. Otherwise, $T$ modulates $M(px_i')$ as the average value of the $k$ highest pixel values of unsigned areas in the sampling image $M$. Since the light distribution of the transformed piece serves as the denominator, the over-exposure as well as under-exposure illumination can be adjusted precisely. Completed by the manipulated pixel value, each of the final pixels is able to approximate the original light degree.

### 2.6. Separating texts from photos

For the signed squares, there are two kinds of objects: text and photo. In this phase, we address separately. First, the simulator $T$ computes the variance of the signed objects ($VA$) one by one from left to right according to the following formula:

$$VA = \frac{1}{n}\sum_{i=1}^{n}(px_i - px_{av})^2. \tag{6}$$


**Fig. 3.** Text 1: left-top under-exposure comparison.

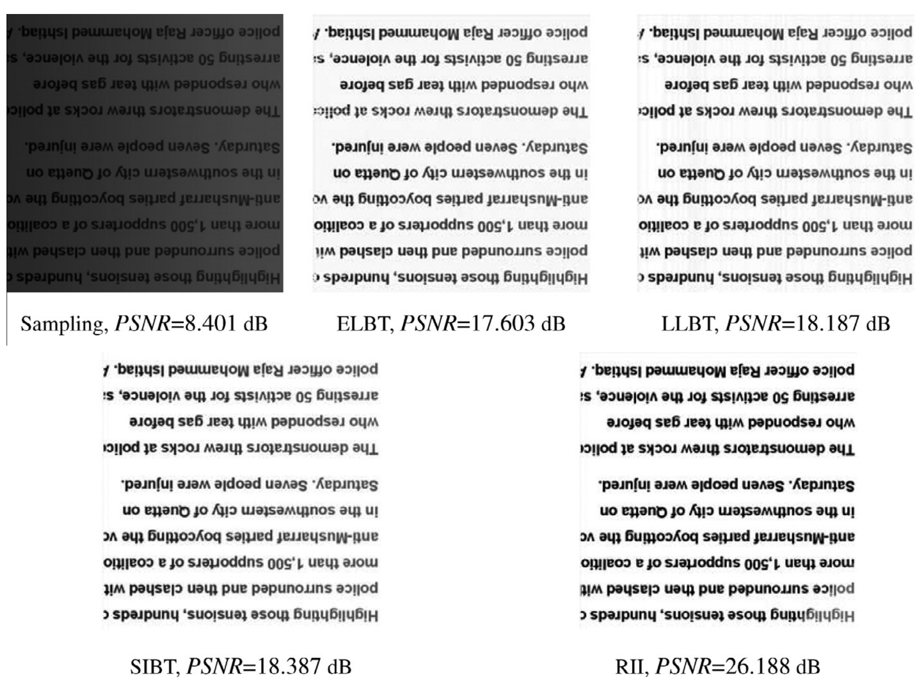


**Fig. 4.** Text 2: all under-exposure comparison.

Note that $n$ is the total number of the pixels in one object, $px_{av}$ is the average pixel value of all the pixels involved in the object, and $px_i$ is the $i$th pixel value.

Next, $T$ computes the average size of all signed objects. Then, $T$ compares the size of the signed objects with the average one. If the size of an object is twice the average size for all objects and $VA < 1500$, then this object is regarded as a photo. Otherwise, $T$ considers it as text. Because the text is always rougher and takes up less space, this can help to figure it out. Even the picture is rough, such as Baboon, it still occupies a larger space than the text objects. By taking into account both size and variance factors, this method can separate text from photos conveniently and efficiently.

Next, $T$ repeats the operations depicted above until all of the signed objects have been defined as either text or photo. In this phase, the photo blocks and text blocks can be distinguished and addressed separately. With over-exposure, the photo blocks are almost the same as the background, while the text blocks are just

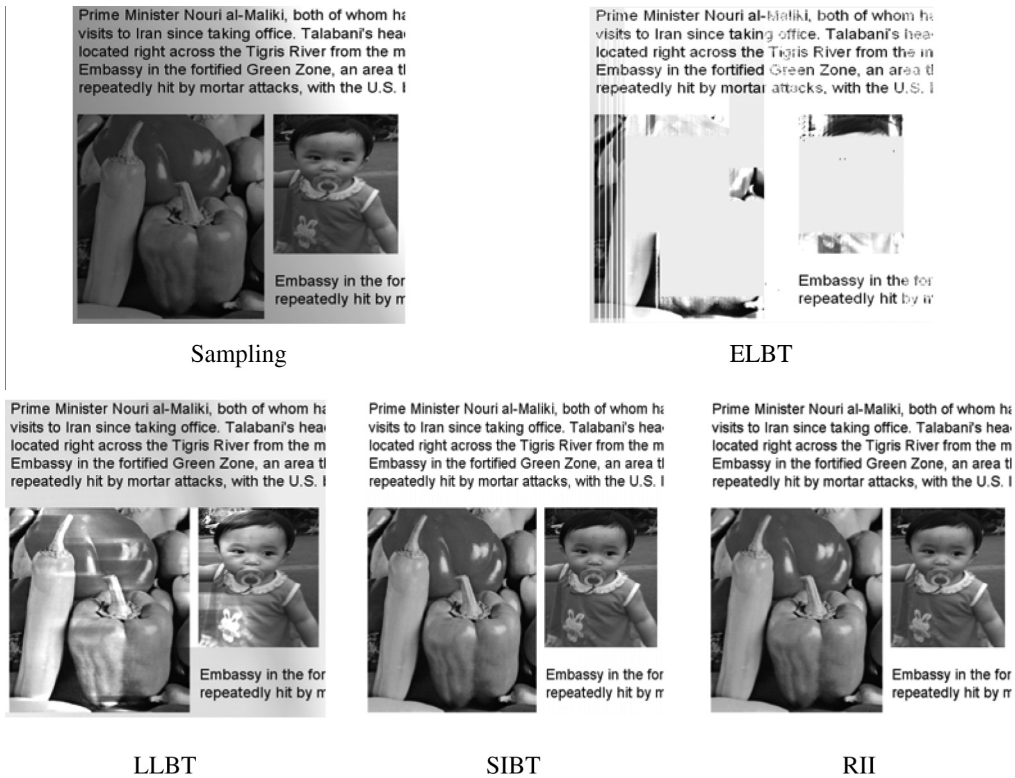


**Fig. 5.** Under-exposure scanned image.

partly white. Consequently, it is impractical to handle the over-exposure pieces using the same strategy for both photo and text as for under-exposures. In the under-exposure archives, the pixel values of the photos are clearly changed; in the over-exposure ones, the background stays nearly white. Considering the different characteristics of these two kinds of blocks under these conditions, we can provide a favorable visual effect by separating these blocks.

### 2.7. Balancing texts

Taking the objects regarded as texts into account, if they are over-exposure, then *T* sorts all pixel values from smallest to largest within the objects. Next, *T* then chooses the lowest *k* pixels and calculates the average value to serve as the replacing pixel value (*RP*). According to the exposure effect, *T* applies the average value of the lowest two-thirds pixel values as the text threshold (*TT*). Within the signed objects, *T* checks all pixels one by one. If $px_i < TT$, then *T* replaces $px_i$ with *RP*; otherwise, the pixel stays the same. If the sampling image *M* is justified as under-exposure in the estimating light degree phase, then *T* can ignore this step.

### 2.8. Balancing photos

Dealing with the signed objects which are estimated as photos, *T* first calculates the average pixel values of all pixels within the objects. Here, the average pixel value is represented as $Ppx_{av}$.

If the sampling image *M* is defined as over-exposure, then *T* judges the final pixels $px'_i$ as follows:

$$px'_i = px_i - (Ppx_{av} - 20)/3, \tag{7}$$

where $px_i$ is the *i*th pixel value in the sampling image corresponding to $px'_i$.

On the other hand, if the original sampling image *M* is regarded as a under-exposure during the estimating light degree phase, then the final pixels is computed as

$$px'_i = px_i + (Ppx_{av} - 20)/2. \tag{8}$$

In this way, the final pixels in the photo part can resist lightening during the process of radiance balancing. Thus, the images can recover the original photo and show the transferred text content clearly.

## 3. Experimental results and discussions

In this section, we demonstrate the optimal effects of the proposed method by conducting essential experiments on under-exposure text images, under-exposure text-photo images, over-exposure text images, and over-exposure text-photo images. We employed the C# language and Intel 2.66 GHz in the experimental environment. To demonstrate practicality, we offer two types of test images: artificial and natural. Figs. 5, 9 and 11–13 are natural sample images, while Figs. 3, 4, 6–8 and 10 are artificial ones. Natural samples were captured by devices; thus, we can assess the effect of each method from human vision. For the artificially simulated pieces, uneven light distribution was created by Photoshop CS5. Accordingly, we are able to evaluate the performance according to the corresponding *PSNR* values and visual perception.

Experiments in Sections 3.1 and 3.2 are for under-exposure images, while those in Sections 3.3 and 3.4 are for over-exposure images, illustrating that the proposed method can deal with both kinds unlike related methods such as ELBT, LLBT, and SIBT. Here, all experimental images are $512 \times 512$ pixels. Furthermore, we provide the results of balancing uneven light distribution for complicated and colorful images in Section 3.5.

As the input images have been divided by the value of *DP* as under-exposure and over-exposure images, the new method is able to

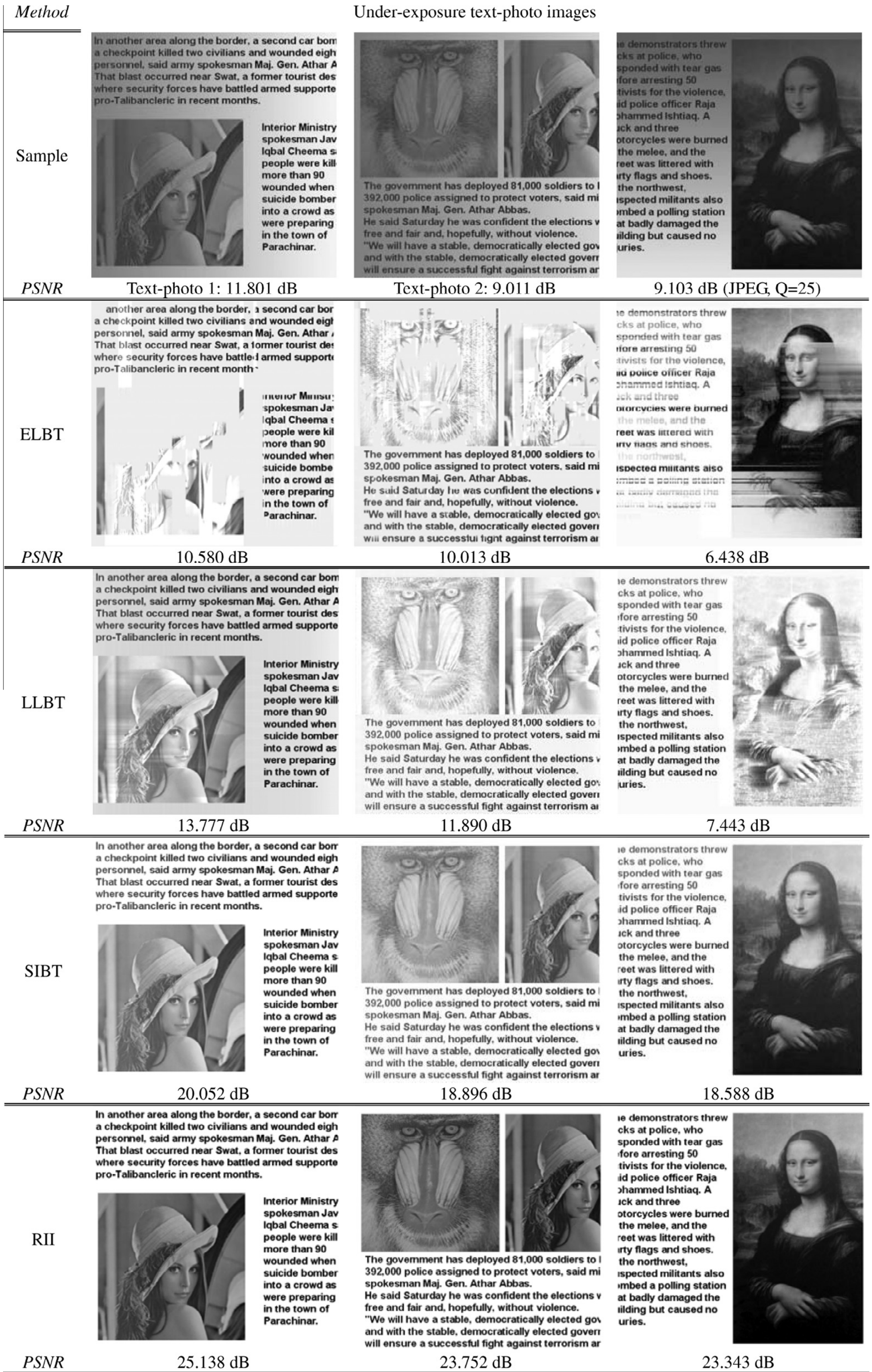


**Fig. 6.** Processing under-exposure text-photo images.

distinguish them and dispose the over-exposure pieces satisfactorily, unlike in other methods. In the experiments, the pre-defined threshold *PT* is set to 45, which allows us to distinguish black from white.

### 3.1. Experiments for under-exposure text images

A text image contains only letters. If it is under-exposure, the letters become difficult to determine. Moreover, the shadow can

**Table 1**
Evaluations of *LDL* values for under-exposure samples.

| | Text 1 | Text 2 | Text-photo 1 | Text-photo 2 |
|---|---|---|---|---|
| Sample | 14,169,699 | 45,297,109 | 15,224,088 | 29,864,170 |
| ELBT | 15,980,288 | 11,396,278 | 1,050,829 | 8,975,078 |
| LLBT | 15,097,858 | 11,722,780 | 12,418,988 | 11,298,237 |
| SIBT | 15,158,689 | 12,074,857 | 1,608,975 | 14,942,972 |
| RII | 182,469 | 165,802 | 214,373 | 291,545 |

come from the left, right, bottom, top or any other direction, so here we list some typical under-exposure images and their processing results with different methods to display the advantage of the proposed method. As shown in Fig. 3, the under-exposure text image is processed by ELBT, LLBT, SIBT, and RII, respectively. It can be seen that the outcome of the RII is much closer to the original image than others according to human vision. To provide a more precise evaluation of these methods, we utilize the peak signal-to-noise rate (*PSNR*) to measure the image quality of these processed images. *PSNR* is calculated as

$$PSNR = 10\log_{10}(255^2/MSE)\mathrm{dB}, \tag{9}$$

where the *MSE* represents the mean square error of an image with $h \times w$ pixels. The definition of *MSE* is

$$MSE = 1/(h \times w)\sum_{i=1}^{h \times w}(p_i - \overline{p_i})^2, \tag{10}$$

where $p_i$ is the original pixel value and $\overline{p_i}$ is processed pixel value within the result.

It is clear that the *PSNR* value of RII is the highest among all processed outcomes, as shown in Fig. 3. Furthermore, taking the different orientations of the shadow into account, we can evaluate the effects of the novel method by its processing outcome, which is displayed in Fig. 4. Both the visual results and *PSNR* values show that the proposed method outperforms related works when dealing with under-exposure images.

Unlike related methods, RII first separates the text and photo sections and then addresses them. As a result, RII is able to improve the text sections by setting a threshold to distinguish characters and background in under-exposure conditions. Then, it deepens these characters relevantly. Therefore, even the SIBT, which has shown optimistic effects on under-exposure images, cannot perform as well as RII due to its lack of handling text sections alone.

### 3.2. Experiments for under-exposure text-photo images

As text-photo images convey much more information than text images, they are more popular in digital archives. Thus, we must evaluate whether the proposed method can work on text-photo images as well as text-only ones. First, RII figures out the text and photo parts according to the variance and size of the signed objects. Then, it can balance the irregular radiance of text and photo parts with different procedures. Therefore, RII can achieve more accurate quality. Note that the setting of $VA < 1500$ depends on the experimental result with various test images, including rough, smooth, and normal ones.

Fig. 5 is a scanned image. The improved outcome of individual method demonstrates that RII is superior to related works in terms of handling the photo sections. Due to the physical character of machines, the under-exposure on the left side can be recovered by SIBT, while the result is too bright on a certain scale. It is clear that by RII, the radiance of photos can meet sufficient balancing, and texts are well restored due to separate handling of the text and photo sections. It is apparent that the recovered image is more friendly from the human visual system.

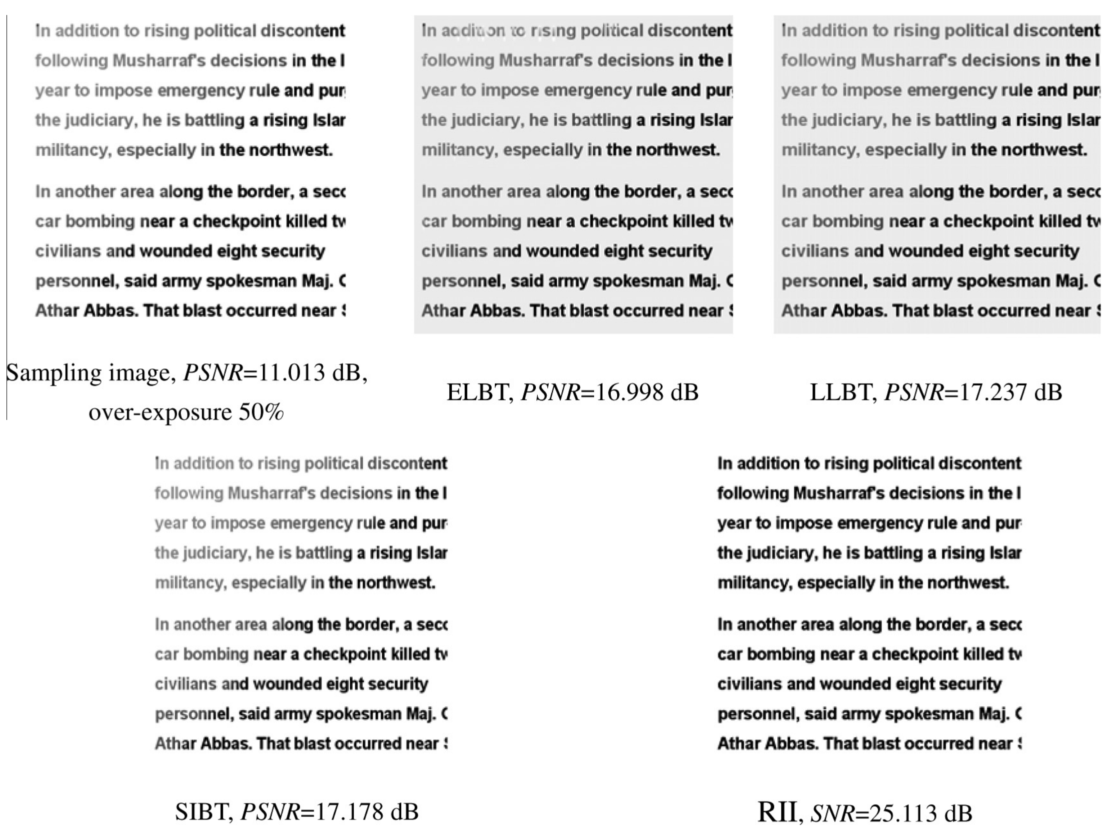


**Fig. 7.** Text 3: processing left-top over-exposure text images.

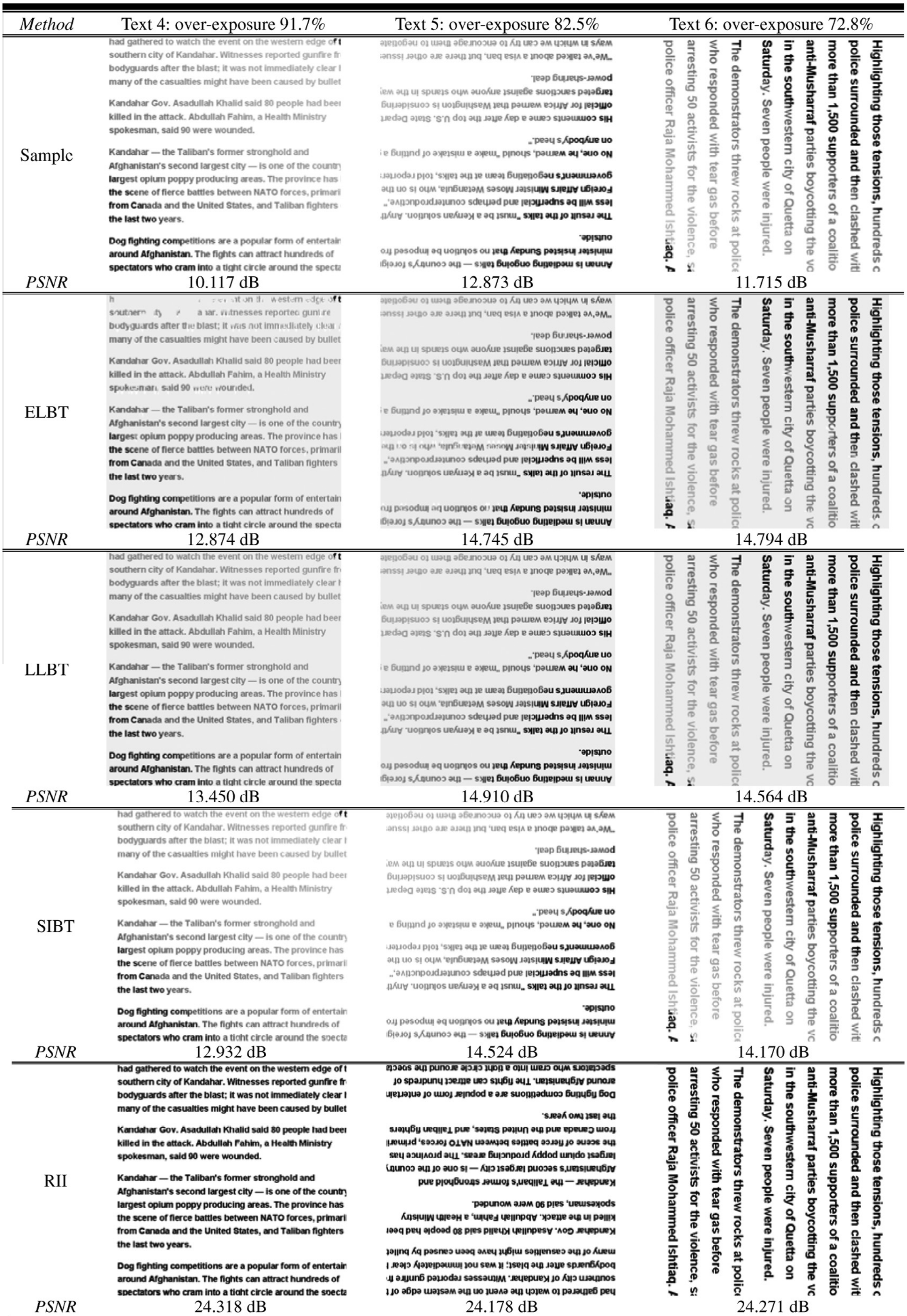


**Fig. 8.** Processing different oriented over-exposure text images.

We use four artificial under-exposure images to demonstrate the effect of RII. As shown in Fig. 6, ELBT is incapable of dealing with the text-photo images, while the LLBT and SIBT, which can recover the original image, show low *PSNR* values.

Because the average pixel value was subtracted by a common under-exposure factor 20 and the outcome was divided by three to balance the radiance distribution of photo, the improved result comes out perfectly and possesses high *PSNR* value. Actually, SIBT also obtains acceptable results in this case. Since RII adopts the Gauss–Laplace detector to help border the edge, while SIBT employs Sobel detector, RII can outperform SIBT by eliminating the noise and guaranteeing that the processed image will be the same

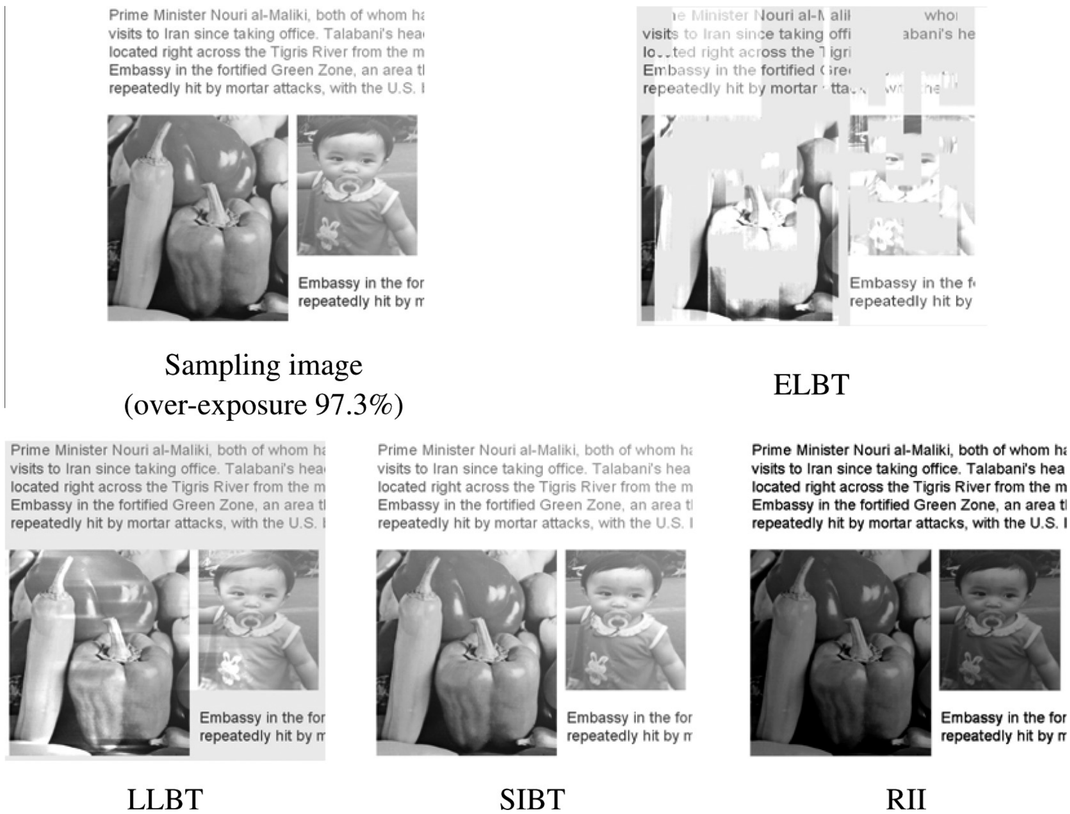


**Fig. 9.** Text-photo 3: over-exposure scanned text-photo images.

in different directions. Thus, RII is able to greatly improve the recovered image quality.

To highlight the functionality of RII, we employ the light drift level (*LDL*) value to evaluate the light distribution of the processed pictures [8]. The *LDL* value is defined as follows:

$$LDL = \sum_{i=0}^{h}\sum_{j=0}^{w}|p_{ij} - mean|,$$
$$mean = \left(\frac{\sum_{i=0}^{h}\sum_{j=0}^{w}p_{ij}}{h \times w}\right), \tag{11}$$

where $p_{ij}$ is the light distribution for the illumination balance processes, and $h \times w$ is the size of sample picture. Considering the light balance performance with the different samples in Figs. 3, 4 and 6, the results of each method are shown in Table. 1. The mean value is calculated before it is subtracted from each pixel. By accumulating the absolute values of the different methods, the light drifting level results are attained. The more balanced light distribution of the picture, the more similarity between each pixel value and the mean value. That is, a smaller *LDL* value shows greater balancing ability for each method. According to Table 1, we can see that the proposed method obtains good balanced results compared with other algorithms. The *LDL* value is more suitable for evaluating the quality of recovered text-only pictures. Although the size of text-photo sample is small, it still works well.

### 3.3. Experiments for over-exposure text images

Considering over-exposure during scanning or other processes, RII still can do well with over-exposure images. For the text images, it is very important that these images regress to the originals in order to determine useful information. As revealed in Fig. 7, the left over-exposure text image with *PSNR* of 11.013 dB can be recovered by RII perfectly, showing the *PSNR* as 25.133 dB. In particular, other methods can not deal with the over-exposure ones.

In addition, we apply over-exposure images with different orientations and distinct ratios of artificial illumination to related works and RII. The balancing results are displayed in Fig. 8. According to visual perception, the result of RII is the much better than those of related works. Furthermore, with the *PSNR* value consistently above 24 dB, RII displays an acceptable resolution for renewing the over-exposure text images.

The main reason that RII can obtain a satisfactory result is that it first determines the illumination of the transformed image referring to its four corner pixels. After a series of processing steps, it separates the signed objects by text and photos. For different signed objects, RII can automatically select corresponding steps to be bolded or deepened them. This gives it a chance to deal with the over-exposure pieces in the archives, which outperforms other existing methods. By successfully balancing the radiance in the background and bolding the content of text, RII can perform efficiently to reveal original information when dealing with over-exposure text images.

### 3.4. Experiments for over-exposure text-photo images

Accounting for the fact that the content of over-exposure text-photo images is difficult to determine, as the photos inside are too bright, here we face a crucial challenge of balancing the uneven light illumination. We employ scanned images as well as artificial ones created by Photoshop to demonstrate the experimental results.

As displayed in Fig. 9, ELBT, LLBT, and SIBT cannot show the original substance clearly when conducting on scanned images. Here,

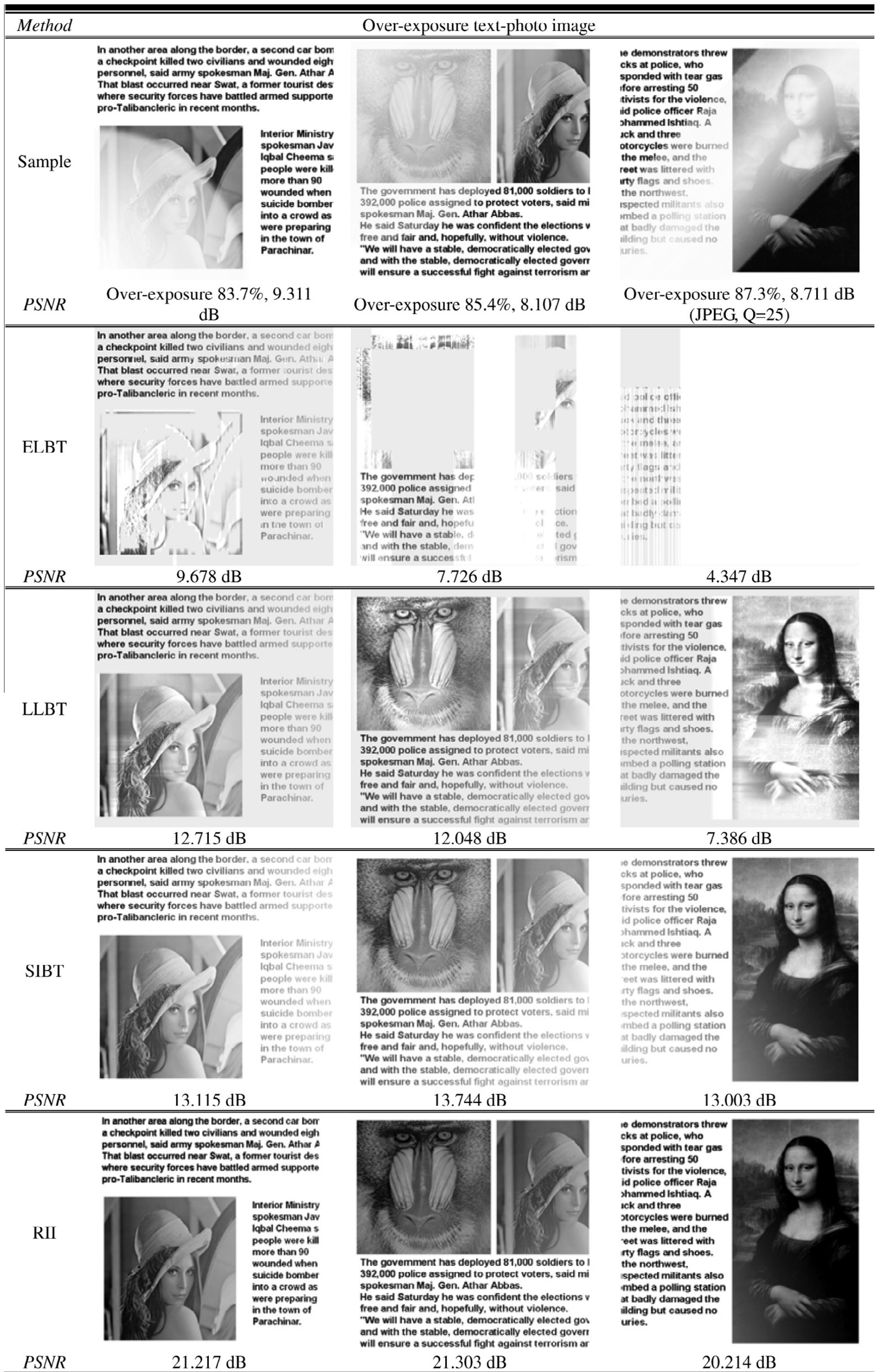


**Fig. 10.** Processing diverse oriented over-exposure text-photo images.

RII can deepen the color of the photos inside and make the texts stand out in order to be read easily. By analyzing the corner pixel values and dealing with the text and photo sections separately, RII can shed light on the original image with high visual quality.

Regarding randomness in nature, we show the results of random direction over-exposure images to estimate the performance of RII. It is apparent from Fig. 10 that ELBT distorts the original image content, while LLBT and SIBT still leave the images

**Table 2**
Evaluations of *LDL* values for over-exposure samples.

| | Text 3 | Text 4 | Text 5 | Text 6 | Text-photo 3 |
|---|---|---|---|---|---|
| Sample | 12,555,658 | 9,174,627 | 12,863,564 | 12,761,448 | 13,191,559 |
| ELBT | 11,686,374 | 8,130,096 | 7,320,666 | 6,585,375 | 4,120,400 |
| LLBT | 11,722,762 | 8,448,387 | 10,085,162 | 8,977,873 | 10,311,043 |
| SIBT | 12,277,401 | 8,820,278 | 12,681,580 | 12,870,912 | 12,855,238 |
| RII | 174,035 | 192,140 | 215,388 | 210,547 | 1,880,392 |

**Table 3**
Comparisons for image performance.

| Performance | ELBT | LLBT | SIBT | RII |
|---|---|---|---|---|
| Edge detection | – | – | 4N | N |
| Signing | – | – | N | N |
| Illumination balance | N | N | N | N |
| CPU time (s) | 4.1 | 4.4 | 4.0 | 3.7 |
| Memory requirement (number of buffer) | 80 | 1/N | 0 | 0 |

over-exposure. As for RII, the photos have been made distinct, and the over-brightness in the text of the sampling images has been eliminated. More importantly, the *PSNR* values of the RII processing are the best among these methods.

Moreover, the *PSNR* for the RII processing is still more than 20 dB, which is enough for humans to make sense of the content of objects. Also, RII can improve the image quality under JPEG attack due to the Gauss–Laplace detection mechanism.

Again, we employ the *LDL* value to estimate the light distribution of each method for handling the over-exposure images. The samples are from Figs. 7–9, and the results are listed in Table 2. It is clear that RII obtains the smallest *LDL* value no matter what test image is utilized, thus proving the superiority of RII in terms of improving over-exposure cases.

To evaluate the performance of RII more clearly, we compare the computational cost for various methods, including the operators in different steps, the CPU time, and the memory requirement. Here, *N* represents the number of pixels within the sample picture, and the CPU used is Intel 2.66 GHz. As SIBT and RII separate the text objects from the photo ones before balancing the irregular illumination, they need 4*N* and *N* operators, respectively, for detecting edges and *N* operators to contour the object; ELBT and LLBT do not consider the photo sections. By using the Gauss–Laplace detector, RII obtains more accurate signing edge detecting results. Thus, the signing process is shorter with fewer mistakes, leading to the short CPU time, as shown in Table 3. Additionally, the proposed method can save much memory space compared with the former methods by employing light-weighted operators to deal with the processing.

### 3.5. Experiments for complicated and colorful images

We also apply RII to balance the irregular light distribution of colorful images. The proposed method can improve the red, green, and blue (GRB) parts in different proportions. The first row of Fig. 11 displays the under-exposure colorful images, and the second row of Fig. 11 offers the improved results by RII. The first row of Fig. 12 shows the over-exposure colorful images, and the second row of Fig. 12 displays the recovered images. Moreover, we employ RII to balance the complicated colorful samples, which contain under-exposure and over-exposure areas simultaneously, as shown in the first row of Fig. 13. Nevertheless, we have to modify the exposure measurement procedure before balancing the target. The original image is divided into $32 \times 32$ non-overlapping blocks, and the assessment of each block depends on three inside squares, $8 \times 8$, $16 \times 16$, and $32 \times 32$. The outcomes of the processed images balanced by RII are displayed in the second row of Fig. 13. According to the results of these figures, it is obvious that RII is capable of solving the problem of irregular light distribution for complicated and colorful images.


**Fig. 11.** The results of balancing under-exposure colorful images.


**Fig. 12.** The results of balancing over-exposure colorful images.

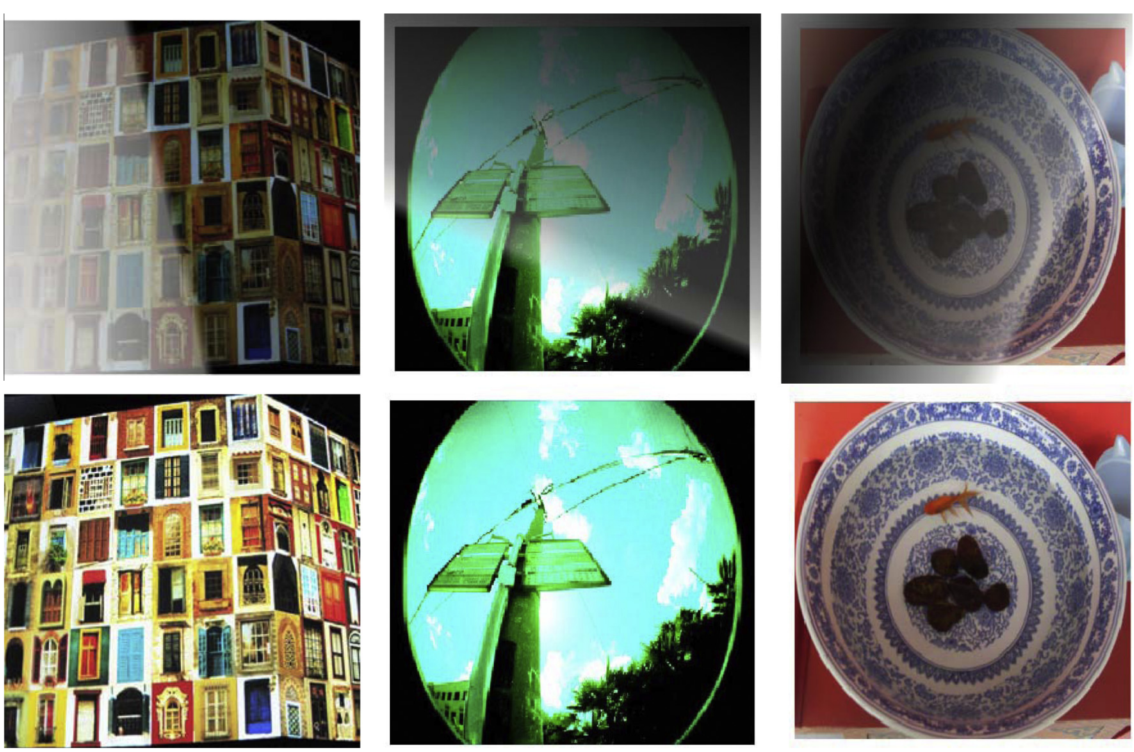

**Fig. 13.** The results of balancing complicated colorful images.

Notwithstanding, one challenge remains: we must spread a white background on the outside of the image when dealing with a complete photo-based image. To eliminate this obstructer so that RII can handle the photo-based image automatically is our future work.

## 4. Conclusions

We propose a novel technique RII to balance the radiance within under-exposure/over-exposure images containing both text and text-photo materials. With the help of the Gauss–Laplace detector and by separating text objects from photo ones, RII can adjust the uneven light distribution of the degraded images, thereby improving the quality of photos and bolding the text content. According to the experimental results, RII outperforms related works in renovating the uneven light distribution. In particular, experiments show that RII can be extended to balance the irregular radiance of complicated and colorful images. In the future, we aim to enhance the quality of the restored image and solve the problem that we need to spread a white background on the outside of the photo-based image.

## References


[1] D. Doermann, J. Liang, H.P. Li, Progress in camera based document image analysis, in: Proceedings of the 7th International Conference on Document Analysis and Recognition, IEEE Computer Society, Edinburgh, Scotland, 2003, pp. 606–616.

[2] J. Liang, D. Doermann, H. Li, Camera-based analysis of text and documents: a survey, Int. J. Doc. Anal. Recognit. 7 (2005) 83–104.

[3] J. Fan, X. Lin, S. Simske, A comprehensive image processing suite for book re-mastering, in: Proceedings of the 8th International Conference on Document Analysis and Recognition, IEEE Computer Society, Seoul, South Korea, 2005, pp. 447–451.

[4] J. Fan, Enhancement of camera-captured document images with watershed segmentation, in: Proceedings of the 2nd International Workshop Camera-based Document Analysis and Recognition, Curitiba, Brazil, 2007, pp. 87–93.

[5] S. Lu, C.L. Tan, Thresholding of badly illuminated document images through photometric correction, in: Proceedings of ACM Symposium on Document Engineering, ACM New York, Manitoba, Canada, 2007, pp. 3–8.

[6] J. Sun, Y. Hotta, Y. Katsuyama, S. Naoi, Low resolution character recognition by dual eigenspace and synthetic degraded patterns, in: Proceedings of the First ACM Workshop on Hardcopy Document Processing, 2004, pp. 15–22.

[7] S.C. Hsia, P.S. Tsai, Efficient light balancing techniques for text images in video presentation systems, IEEE Trans. Circuits Syst. Video Technol. 15 (8) (2005) 1026–1031.

[8] S.C. Hsia, M.H. Chen, Y.M. Chen, A cost-effective line-based light-balancing technique using adaptive processing, IEEE Trans. Image Process. 15 (9) (2006) 2719–2729.

[9] S. Lee, C.H. Chen, C.C. Chang, A novel illumination-balance technique for improving the quality of degraded text-photo images, IEEE Trans. Circuits Syst. Video Technol. (2009) 900–905.

[10] N. Kazakova, M. Margala, N.G. Durdle, Sobel edge detection processor for a real-time volume rendering system, in: Proceedings of International Symposium Circuits System, vol. 2, IEEE Computer Society, Canada, 2004, pp. II913–II916.

[11] Z. Hua, Y. Li, J. Li, Image segmentation algorithm based on improved visual attention model and region growing, in: Proceedings of the 6th International Conference on Wireless Communications Networking and Mobile Computing (WiCOM), IEEE Computer Society, 2010, pp. 1–4.

[12] J.B.T.M. Roerdink, A. Meijster, The watershed transform: definitions, algorithms and parallelization strategies, Fundam. Inf. 41 (2001) 187–228.

[13] M.J. Taylor, C.R. Dance, Enhancement of document images from cameras, in: Proceedings of the 5th SPIE Conference on Document Recognition, Vol. 3305, CiteSeer, 1998, pp. 230–241.

[14] J. Fan, A local orientation coherency weighted color gradient for edge detection, in: Proceedings of IEEE International Conference on Image Processing, IEEE Computer Society, 2005, pp 1132–1135.